SENSITIVITY ANALYSIS ON TRIAXIALITY FACTOR AND LODE ANGLE IN DUCTILE FRACTURE

Ghajar R.

Mechanical Properties Research Lab (MPRL)
Faculty of Mechanical Engineering
K.N. Toosi Univeristy of Technology, Tehran, Iran

Mirone G.

Facoltà di Ingengeria
Università di Catania
Catania, Italy

Keshavarz A. *

Mechanical Properties Research Lab (MPRL)
Faculty of Mechanical Engineering
K.N. Toosi Univeristy of Technology, Tehran, Iran

ABSTRACT

Accuracy of numerical analysis is always important but it is much more important in failure analysis of ductile materials. In ductile materials, the process of removing the effects of necking to obtain stress-strain curve usually need reverse identification methods which are based on iterative finite element analysis. Moreover, triaxiality factor and Lode angle (two parameters that control failure of ductile materials) are obtained from finite element analysis.

In this article based on some experiments, the effect of triaxiality factor and Lode angle on the failure strain of *X*100 pipeline steel is studied. In order to gain a better understanding of the response of triaxiality and Lode angle to deviations of stress, a sensitivity analysis is done on these two parameters before the start of finite elements (*FE*) analysis. This sensitivity analysis shows that the two parameters are really sensitive to stress deviations in some areas. Three geometries are selected and their *FE* analysis shows that it is necessary to reduce the element size lower than what is reported in literature in order to get convergence in triaxiality factor and Lode angle in critical areas.

Keywords: Triaxiality factor, Lode angle, Failure strain, Sensitivity analysis.

1. INTRODUCTION

From the experiments done by Bridgman [1], it is known that hydrostatic stress has some effect on failure of ductile materials. Recently some researches have shown that not only hydrostatic stress, but also another factor which is related to the third invariant of deviatoric stress tensor has some effects on ductile failure. The effect of hydrostatic stress is embedded in triaxiality factor (*TF*) and the effect of third invariant of deviatioric stress tensor is shown by Lode angle (*X*). Lemaitre [2], Lemaitre *et al*. [3], Chaboche [4] and Bao [5] are samples of those researches that are based on only *TF* and Xue and Weirzbiki [6], Bai and Wezrzbicki [7], Gao *et al*. [8] and Mirone and Corallo [9] are samples of those researches that take into account both factors. It is clear that it is not possible to develop a failure model with these parameters without the help of numerical analysis, because the only information that can be extracted from experiments are the load applied by the testing machine and the displacements. Therefore; the use of numerical analyses for determining *TF*, *X* and other material parameters is mandatory. However, when the material parameters are extracted from a mixed numerical-experimental analysis and the analyses are severely nonlinear (large deformation elasto-plastic analysis), it is really necessary to pay special attention to the accuracy of numerical results. Moreover in the numerical analysis it is seen several times that by a small change in controlling parameters of finite element analysis, the values of these two parameter and specially Lode angle change a lot.

In this article, in order to show the effect of *TF* and *X* on the failure, the results of a series of experiments are presented that shows the failure strain of *X*100 steel is sensitive to both *X* and *TF*. Then a sensitivity analysis on *X* and *TF* is done in order to study the effects of errors in each principal stress on these two parameters. Due to application of this metal, positive *TF* and especially first quadrant of *X*-*TF* is studied.

The results of this sensitivity analysis show that in some cases, if there is a small error in calculating stresses, there will be a much bigger error in calculating *X* and *TF* and because of this effect in some cases it is

* Corresponding author (a_keshavarz@dena.kntu.ac.ir)

DOI : 10.1017/jmech.2012.125
Copyright © 2013 The Society of Theoretical and Applied Mechanics, R.O.C.
https://doi.org/10.1017/jmech.2012.125 Published online by Cambridge University Press

really mandatory to decrease the element size in failure area to 50μm.

2. FAILURE PARAMETERS

If σ_{ij} is the stress tensor, then principal stresses are shown by σ_1, σ_2, σ_3 that $\sigma_1 \geq \sigma_2 \geq \sigma_3$. According to the models that are developed for plasticity and failure, it is preferred to use some other factors that have common usage in this field of study such as triaxiality factor and Lode angle instead of working directly with principal stresses.

It is always possible to write the stress tensor as a summation of a radial tensor with equal components, which is called mean stress tensor, and a deviatoric tensor, as shown in Eq. (1).

$$\sigma_{ij} = \sigma_m \delta_{ij} + \sigma'_{ij} \tag{1}$$

σ_{ij}, σ_m, δ_{ij} and σ'_{ij} are stress tensor, mean stress, Kroneker Delta and deviatoric stress tensor, respectively.

TF which is defined as the ratio of mean stress to equivalent stress, σ_{eq}, is a parameter that shows whether the state of stress is near to mean stress tensor or not and its sign shows whether the mean stress tensor is compressive or tensile. It ranges $[-\infty, +\infty]$ and very big values are related to the states of stress near to (σ, σ, σ) and the sign is the same as the sign of σ. More details about different values of *TF* can be found in [9].

$$TF = \frac{\sigma_m}{\sigma_{eq}} \tag{2}$$

In a stress space, it is possible to define a hydrostatic line ($\sigma_1 = \sigma_2 = \sigma_3$). The projection of the state of stress to this line, gives mean stress and the distance between state of stress and the hydrostatic line gives equivalent stress. Another parameter is defined as the angle between the line, which connects the state of stress to its projection on hydrostatic line, and a reference line. The reference line is σ'_1 axis and the angle, θ, is called Lode angle. This angle shows that whether the state of stress is near to axisymmetric stress state or plane stress state [10]. The Lode angle is related to deviatoric principal stress components and the geometrical representation of Lode angle is shown in Fig. 1.

It is possible to find the relation between Lode angle and third invariant of deviatoric stress tensor. This relation is shown in the following equation [7].

$$X = \cos(3\theta) = \frac{27 J_3}{2\sigma_{eq}^3} \tag{3}$$

In literature, the parameter *X* sometimes is used as the Lode angle parameter, as it is done in this article.

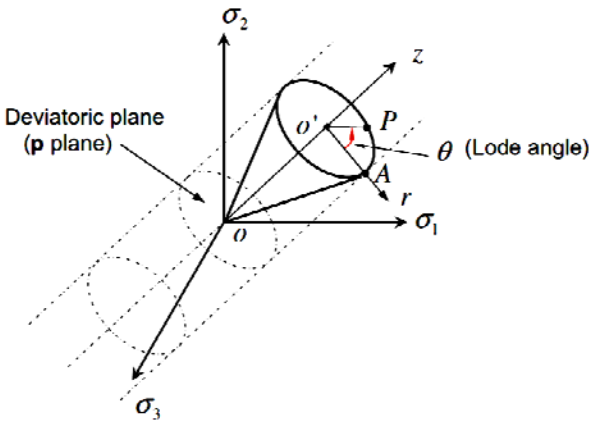


Fig. 1 Lode angel θ in principal stress space, P: stress state, Oz: hydrostatic axis, O'r: σ'_1 axis [7]

A more detailed explanation about *X* parameter is given in an article by one of the authors [9]; "*X* ranges in [−1, 1] and is equal to 1 for stress states of the kind $(\sigma_A, \sigma_B, \sigma_B)$ with $\sigma_A > \sigma_B$, to zero for principal stresses like $(\sigma_A, \sigma_B, (\sigma_B + \sigma_A)/2)$, and to −1 for $(\sigma_A, \sigma_B, \sigma_B)$ with $\sigma_A < \sigma_B$; the first of these three stress states is typical of the center of axisymmetric structures axisymmetrically loaded in tension and includes the uniaxial tension as a particular case when $\sigma_B = 0$ or pure hydrostatic tension when $\sigma_A = \sigma_B$, the second is a generic plastic plane strain state and includes the pure shear as a special case with $\sigma_A = -\sigma_B$, the third corresponds to axisymmetric compression and degenerates in uniaxial compression when $\sigma_B = 0$ or pure hydrostatic compression when $\sigma_A = \sigma_B$".

3. EFFECT OF *X* AND *TF* ON FAILURE

Basically, ductile fracture consists of three steps which are void initiation, void growth and void coalescence. In most of the alloys, void initiates in early stages of plasticity, grows in later stages and finally coalescence causes a small crack to create. This small crack grows and breaks the specimen into 2 or more parts.

When *TF* increases, the process of growth and coalescence becomes faster and the specimen fails in a lower strain. Lode angle has some effect on void growth and mainly coalescence. When this parameter decreases from 1 to 0, voids tend to elongate during growth and shear-off in coalescence. More detailed explanation about the effect of Lode angle, in micro and macro scale, is given in references [11,12].

In order to show the effect of *X* and *TF* on failure, the results of some experiments are used which include tensile tests on smooth and notched round bars [13], tensile tests on flat notched specimens [14] and torsion test on smooth round bar [15] cut from *X*100 pipeline steel. The first two groups of experiments are done with a tensile testing machine under static loading with speed of 1mm/min. Two cameras and a clip gage are used to measure the deformations. More details about the torsion test can be found in [15].

https://doi.org/10.1017/jmech.2012.125 Published online by Cambridge University Press

The stress-strain curve used in this research is obtained from the experimental true stress-true strain curve of smooth round bars (9mm diameter, 55mm gage length), corrected through the MLR function [16] which eliminates the necking-induced triaxiality from the true stress and takes into account the departure between true stress and equivalent stress in the post-necking strain range. The experimental true stress and the corrected stress are reported in Fig. 2. Also the results of tensile experiments on round notched bars (9mm diameter, 6mm minimum diameter, 2 and 10mm notch radius, *R*2 and *R*10 respectively) are given in Figs. 3 and 4.

From the above experiments and *FE* analysis, X and TF values at failure points are extracted during the loading and the average X and TF are calculated according to Eqs. (4) and (5). The *FE* analyses are done using commercial code MSC Marc software. Large deformation in the framework of updated Lagrangian and implicite integration are used in analysis. Time steps are in the range of 0.002 ~ 0.005. A subroutine is added to calculate TF, X, TF_{avg} and X_{avg}. Eight node brick element is used for grid generation of flat specimens and four node axisymmetric elements for round specimens in tension. Possible symmetries are used to reduce computational costs and displacement conditions are imposed for simulating testing machine crosshead motion. In each specimen, analysis continues until load and deformation becomes equal to those extracted from experiments in failure then in this step the average values in the failure location is reported as failure parameters' values for the specimen.

Failure point in all the above mentioned specimens under tension (round and flat) is the central point of minimum cross section. In the above mentioned round bars in tension, Lode angle is always one in failure point and triaxiality changes. According to the X_{avg} and TF_{avg} values at failure in smooth and notched round bars, a failure curve is proposed which is shown in Eq. (6). Moreover, different flat and round notched specimens are tested for the same material in another research [14], by the authors, shows that X does not affect the failure strain in high triaxialities, $TF_{avg} = 0.85 - 1.7$, and the smallest TF_{avg} related to a flat notched specimen *FN*-10, the geometry is shown in Fig. 5 and dimensions in Table 1, is 0.85 with failure strain of 1.25. A similar result is extracted for other materials in [9,17]. Therefore, Eq. (6) is correct for $TF_{avg} \geq 0.85$ regardless of the value of X_{avg}. In order to check the effect of X on the failure, the result of pure torsion test ($\varepsilon_{failure} = 1.27$) from [15] is added here. From *FE* analysis both X_{avg} and TF_{avg} are equal to zero at failure. The list of the failure points of the specimens is given in Table 2.

$$\int_0^{\varepsilon_{eq}} TF \, d\varepsilon_{eq} = \varepsilon_{eq} \cdot TF_{avg}(\varepsilon_{eq}) \tag{4}$$

$$\int_0^{\varepsilon_{eq}} X \, d\varepsilon_{eq} = \varepsilon_{eq} \cdot X_{avg}(\varepsilon_{eq}) \tag{5}$$

$$\varepsilon_f(TF_{avg}, 1) = 2.48 \ \exp(-0.836 \ TF_{avg}) \tag{6}$$

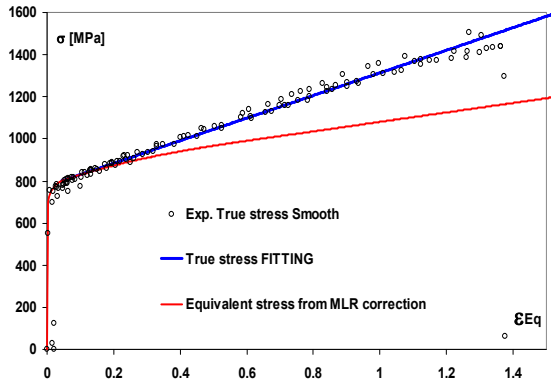


Fig 2 True stress-true strain curve for smooth round bar specimen [13]

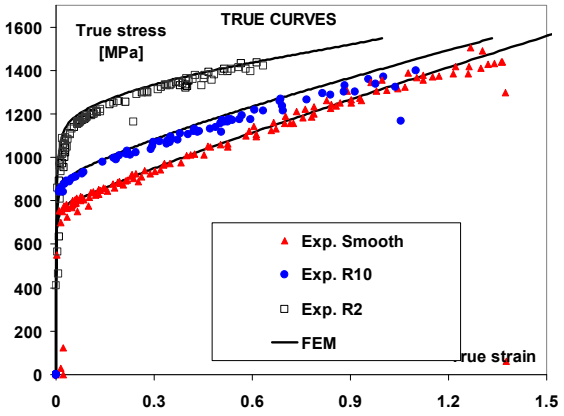


Fig. 3 True strain-true stress curves for round bars [13]

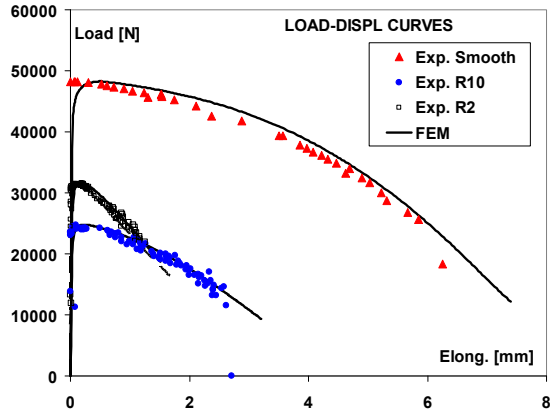


Fig. 4 Load-displacement curves for round bars [13]

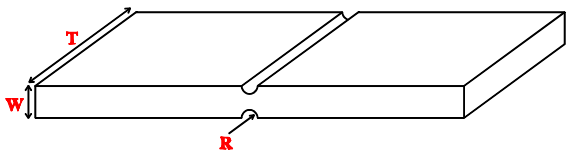


Fig. 5 General geometry of *FN* specimens

https://doi.org/10.1017/jmech.2012.125 Published online by Cambridge University Press

Table 1 List of flat notched specimens according to Fig. 5

Specimen name	W	Min. W (@ notch section)	R	T
FN-10	16	7	2	6
FN-11	8	4	1	13
FN-14	8	3.5	4	13
FN-17	8	3.5	2	13

Table 2 Failure points used in calibration of failure criterion

specimen	TF_{avg}	X_{avg}	ε_f
Smooth round[1]	0.73	1	1.35
R-2[1]	1.69	1	0.61
R-10[1]	1	1	1.05
Torsion[2]	0	0	1.27
FN-10[2]	0.85	0.56	1.25

1. Used in calibration of upper bound.

2. Used in calibration of lower bound.

The failure model proposed here is based on the general failure models in [10,18]. According to these failure criteria, failure strain is a series of exponential curves in failure strain-average *TF* plane that each curve is related to a X_{avg} and the upper curve is for $X_{avg} = 1$ and the lower curve is for $X_{avg} = 0$. These curves are related to each other based on a power law function. In *X*100 material, the upper bound and the lower bound are the same for $TF_{avg} \geq 0.85$ (according to [14]) and after that the lower curve is calibrated using the data of the round bar in torsion and the flat notched specimen. The completed failure criterion is given in Eq. (7), shown in Fig. 6 and the parameters are listed in Table 3.

$$\varepsilon_f = C_1 \exp(-C_2\, TF_{avg}) - \{C_1 \exp(-C_2\, TF_{avg}) - C_3 \exp(-C_4\, TF_{avg})\}(1 - X_{avg}^{1/n})^n \; H(0.85 - TF_{avg}) \tag{7}$$

In the above equation n is the hardening exponent in stress-strain curve and H is the Heaviside step function which is zero for $TF_{avg} > 0.85$ and one for $TF_{avg} \leq 0.85$. From failure criterion it can be seen that, increasing TF_{avg} decreases failure strain and decreasing X_{avg} decreases failure strain in $TF_{avg} < 0.85$.

4. SENSITIVITY ANALYSIS

According to the explanation in introduction section, a sensitivity analysis on *X* and *TF* is done in order to study the effects of errors in each principal stress on these two parameters. Therefore, variations of these two parameters are given in the following equations.

Table 3 Parameters of failure criterion

C_1	C_2	C_3	C_4	n
2.480	0.836	1.270	0.011	0.170

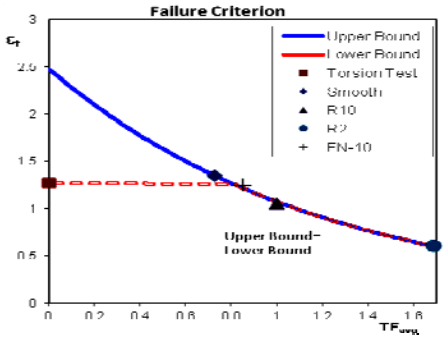


Fig. 6 Failure points of specimens and failure curve

$$\delta TF = \frac{\partial TF}{\partial \sigma_1}\delta\sigma_1 + \frac{\partial TF}{\partial \sigma_2}\delta\sigma_2 + \frac{\partial TF}{\partial \sigma_3}\delta\sigma_3 = TF_{,1}\,\delta\sigma_1 + TF_{,2}\,\delta\sigma_2 + TF_{,3}\,\delta\sigma_3 \tag{8}$$

$$\delta X = \frac{\partial X}{\partial \sigma_1}\delta\sigma_1 + \frac{\partial X}{\partial \sigma_2}\delta\sigma_2 + \frac{\partial X}{\partial \sigma_3}\delta\sigma_3 = X_{,1}\,\delta\sigma_1 + X_{,2}\,\delta\sigma_2 + X_{,3}\,\delta\sigma_3 \tag{9}$$

According to the above formulation, by calculating the derivatives, the amount of sensitivity of each parameter to a change in principal stresses is calculated. As explained in introduction, according to the application of *X*100 pipeline steel, this study is devoted to positive *TF* values. Whereas $TF \geq 0$, $\sigma_1 > 0$. From this point on, in order to make the analysis general, it is assumed that the stresses are normalized with respect to the first principal stress, σ_1, that has a positive value; accordingly the new state of stress is written as $(1, \sigma_2^n, \sigma_3^n)$ that $-1 \leq \sigma_2^n \leq 1$ and $-2 \leq \sigma_3^n \leq 1$.

As the first attempt, we study the case in which all the variations of the principal stresses are equal. In this situation, the variation of *X* is zero, which means; if all the principal stresses in an analysis have the same deviation from the real value, there is no error in calculating the Lode angle. For studying the effect of stress variations on triaxiality, the diagram of its derivative is shown in Fig. 7.

As can be seen in this diagram, up to some values of stresses, the triaxiality derivative is less than one and in this area, there is a damping in errors, but after that, the derivative increases and when the second and third stress are half of the first stress, the derivative reaches the value 2, which means if by any reason there exists an error in a point with these stresses, then the error in triaxiality would be twice. It is worth mentioning that the amount of triaxiality in this point is 1.33.

After studying the above special case, in this paragraph every single derivative is studied to see the effect of each of them. Therefore; general 3D graphs of each of the derivatives in Eqs. (8) and (9) are plotted (*x* axis: σ_2^n, *y* axis: σ_3^n and *z* axis: A derivative) and a

https://doi.org/10.1017/jmech.2012.125 Published online by Cambridge University Press

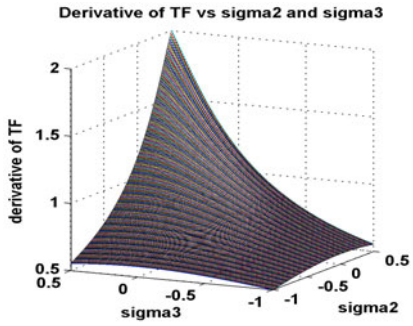


Fig. 7 $\partial TF/\partial\sigma$ for $\sigma_1 = 1, -1 \le \sigma_2 \le 0.5, -1 \le \sigma_3 \le 0.5$

series of sections of these 3D drawings are prepared as 2D plots. In these sections, σ_3^n has −1, −0.5, 0.0, 0.25 and 0.5 values (related to each branch in 2D diagrams) and σ_2^n varies from −1 to 1. The diagrams are shown in Fig. 8 for all the derivatives.

In $X_{,1}$ diagram all the values for $\sigma_3^n = -1$ are less than 1 and also the value for $\sigma_3^n = -0.5$ at the peak is less than 1.5 which means for these values there is not a severe amplifying effect; but the derivative increases for other values of σ_3^n, from 2 up to 4 at the peak and these effects can be seen in the positive values of σ_2^n and mainly $0.5 \le \sigma_2^n \le 1$. The amplifying effect in $X_{,2}$ is more intense compared to that in $X_{,1}$, and in the diagram of $X_{,2}$, the values for $\sigma_3^n = -1$ branch goes lower than −1.5 and in higher values of σ_3^n, $X_{,2}$ decreases so that in $\sigma_3^n = 0.5$ branch, it goes up to 2.5 around $\sigma_2^n =$ 0.3 and it goes down to near −7 around $\sigma_2^n = 0.75$. In the plot of $X_{,3}$, the variations have a large span and in the higher values of σ_3^n, it changes between −4 and 4. The new point in this diagram is that in negative σ_2^n, the values of $X_{,3}$ goes down to −3 while in the two previous diagrams, the values of derivatives were mainly around 1 in negative σ_2^ns.

In the diagrams of derivatives of *TF*, the values of all the branches are less than 1 for negative values of σ_2^n, but in $TF_{,1}$ the values goes lower than −2.5 for $\sigma_3^n = 0.5$. The same situation can be seen in diagrams of $TF_{,2}$. In $TF_{,3}$, the branch of $\sigma_3^n = 0.5$ goes up to 4 and that of $\sigma_3^n = 0.25$ goes up to near 2 and the peak in other branches is less than 1. Compared to the values calculated for derivatives of Lode angle, these values are smaller and critical situation related to high values of σ_3^n.

A good way for getting an immediate insight of how critical is a combination of failure parameters with respect to its sensitivity to stress variations, is that of identifying the areas on the *X*-*TF* plane corresponding to a given sensitivity level, for different values of σ_{eq}^n (normalized equivalent stress).

The derivatives in Eqs. (8) and (9) and *X* and *TF* values are calculated for different combinations of σ_2^n and σ_3^n. These combinations of σ_2^n and σ_3^n are a grid on σ_2^n − σ_3^n plane with 200 points along each

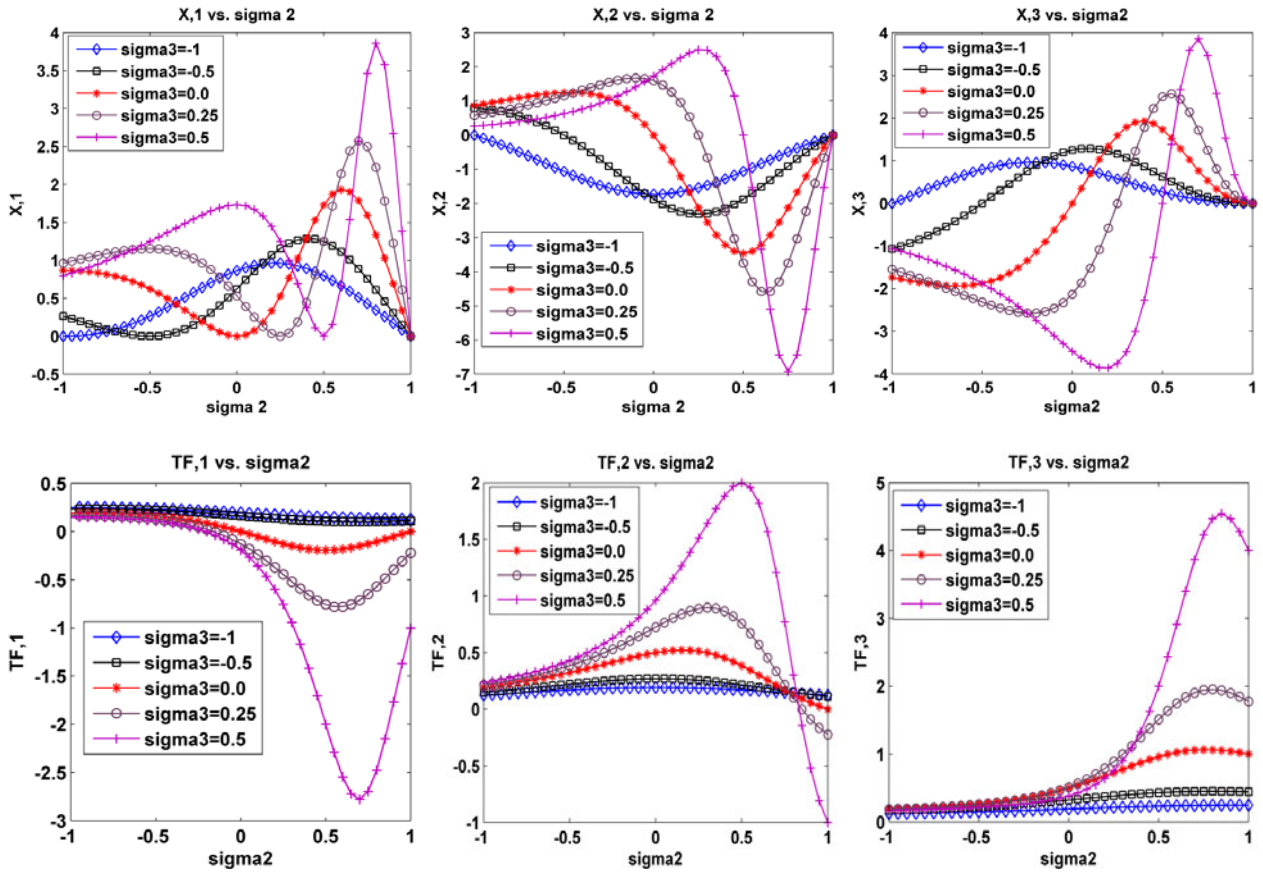


Fig. 8 Derivatives of *X* and *TF* with respect to three principal stresses versus σ_2 for $\sigma_1 = 1$, $\sigma_3 = -1, -0.5, 0.0, 0.25, 0.5$

https://doi.org/10.1017/jmech.2012.125 Published online by Cambridge University Press

axis. The points with sensitivity higher than 2 (derivatives greater than 2), are selected and plotted in Fig. 9. These points are grouped according to σ_{eq}^{n} included in different ranges within the interval [0,2]. The points on the boundary of each area give a sensitivity of two; the points within the area have sensitivity as greater than two as far from the boundary they are. At the centroid of each area, the sensitivity is the maximum possible for that level of equivalent stress. It should be noted that the diagrams of $X_{,2}$ and $X_{,3}$ are the same; also those of $TF_{,2}$ and $TF_{,3}$.

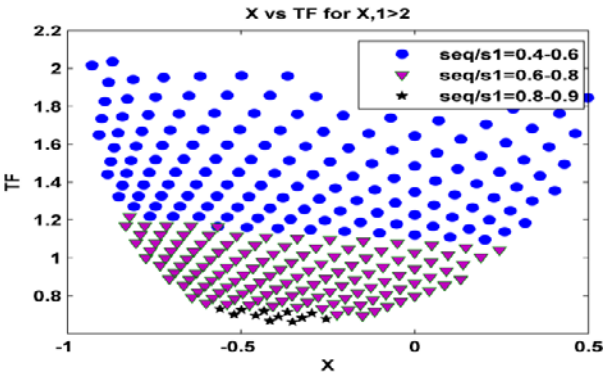
It is visible that the ratio between the equivalent stress and the first principal stress strongly controls the sensitivity: High values of σ_{eq} / σ_1 bring small critical areas, and vice versa. As the above ratio increases, the critical areas tend to move downward and to become smaller.

Our range of interest is the positive quadrant of the *X-TF* plane up to maximum triaxialities of about 1.5: When the ratio σ_{eq} / σ_1 is greater than 0.7, the sensitivity of *TF* to principal stress is lower than 2 all over the field of interest. At the same time, when the equivalent stress is close to 70% of the 1st principal stress, the critical areas for the sentitivities of *X* to σ_2^n and σ_3^n, cover large and slightly inclined bands of the *X-TF* plane, placed in the upper part of our field of interest. As σ_{eq} / σ_1 increases, the critical zones move toward the lower part of the *X-TF* quadrant, and their size reduces and when $\sigma_{eq} = 1.5\sigma_1$, the critical area for the sensitivity of *X* to σ_2^n and σ_3^n, is a tiny short stripe close to the pure shear condition.

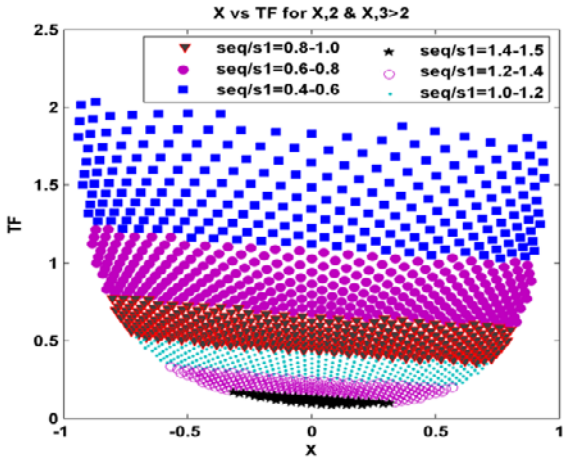
So, in *FE* analyses of failure studies, which is large deformation elastoplastic analysis and highly nonlinear, the variation of these parameters must be checked carefully. For example in mesh sensitivity and step size sensitivity analysis, difference in principal stresses of 5% is acceptable, but as shown in this section, this difference may cause a much bigger difference in *X* and *TF*. Whereas these two parameters are used in failure analysis model development, this change is a source of big error in failure parameters. The numerical analysis done in next section, confirms this reality.

5. DISCUSSION ON SENSITIVITY

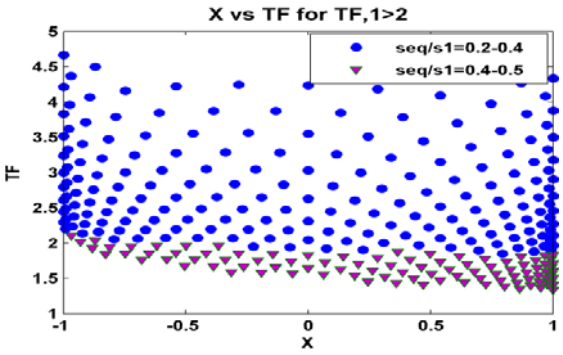
Up to now, the critical areas in *X-TF* plane are identified. In the analysis of each specimen, possible failure points should be checked and if their path crosses critical areas, then a special attention should be paid to element size and step size. In order to study the results obtained in sensitivity analysis, 3 flat notched specimens (*FN*-11, *FN*-14 and *FN*-17) are analyzed using finite elements with several different mesh sizes in the failure area. *FE* analysis is done in the same way that explained in section (3) and due to symmetry only one-eighth of the specimens are modeled. The relevant symmetry conditions are applied to symmetry planes and displacement condition is applied to model the testing machine cross head motion. These specimen and their dimensions are shown in Fig. 5 and Table 1.



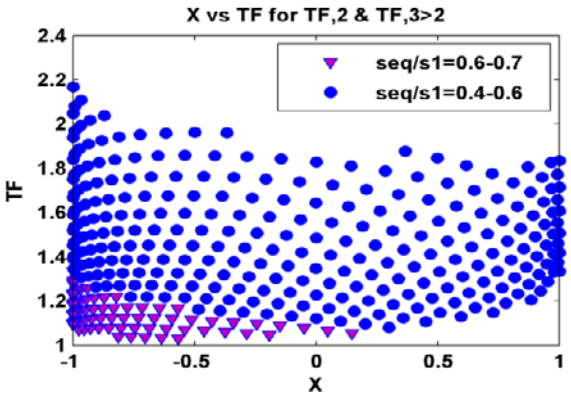
(a)



(b)



(c)



(d)

Fig. 9 Areas with derivatives greater than 2 on *X-TF* plane

https://doi.org/10.1017/jmech.2012.125 Published online by Cambridge University Press

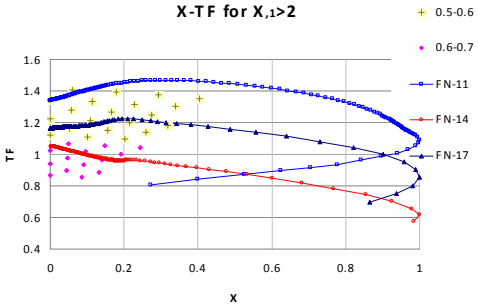
Generally, in *FE* analysis, element sizes are compared to geometrical dimensions of specimen and it is not usual to mention element size, but in *FE* analysis of failure studies, the size of element in failure area regardless of geometrical dimensions becomes important because elements are going to be removed after failure of each element. In literature, element dimensions of order 100 ~ 200μm is accepted for failure studies which is compatible with dimension of unit cell used in studies. In analysis of *FN* specimens the reduction of element sizes continued up to 100 ~ 200μm in failure area and the mesh size effect changes from moderate to high for these geometries.

Then, a check is made for assessing if the three simulated strain histories enter areas of the *X-TF* plane where a special sensitivity of the stress state parameters occurs.

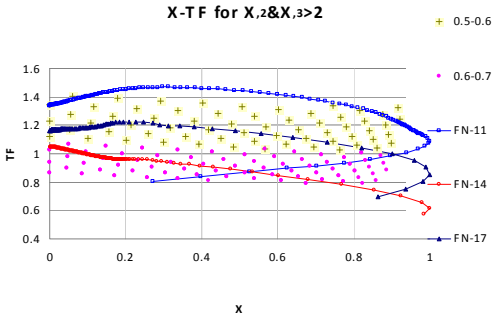
The ratio σ_{eq} / σ_1 for the failure points in the *FN* specimens, analyzed here, lies within the range 0.5 – 0.7 almost all over the strain histories of the three specimens. In Fig. 10 the paths of *X* and *TF* for the failure points of the specimens are reported, together with the area plots indicating the critical area where the sensitivity of *TF* and *X* to variations of the stress components is greater than 2 during the straining history. As mentioned in sensitivity analysis section the diagrams of $X_{,2}$ and $X_{,3}$ are the same; also those of $TF_{,2}$ and $TF_{,3}$.

Figure 10 indicates that *FN*-17 specimen enters critical areas in almost all diagrams and most of its loading history is in areas with sensitivity higher than 2.

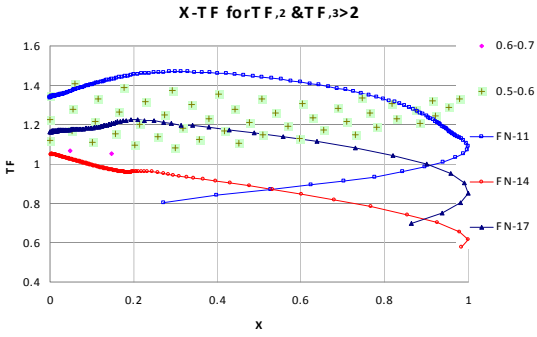
Specimen *FN*-14 enters the critical areas in derivatives of *X* and this means; this specimen in most parts of its loading history is prone to errors in *X*, while specimen *FN*-11, in very limited parts of its history passes through critical areas. Another set of *FE* analysis with element size of 50μm in failure areas of all specimens and one extra on *FN*-14 and *FN*-17 with element size of 30μm are done. According to these analysis, convergence of *FN*-11 can be achieved with element size of 100 ~ 200μm and *FN*-14 and *FN*-17 analysis converges with element size of 50μm, while in other studies on failure [19] and [20], it is reported that element size of 200μm is sufficient for transferability of micromechanical failure parameters for the same material used for modeling in this paper. The *FE* mesh and *FE* results at convergence are given in Fig. 11 and Table 4. This shows that, there are some failure areas which are detected through sensitivity analysis that needs very fine mesh to get reliable results.



(a)

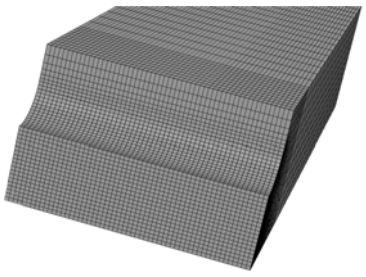


(b)

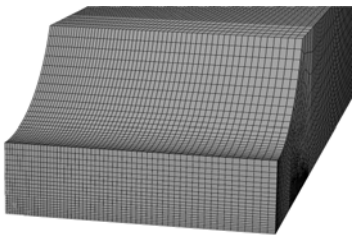


(c)

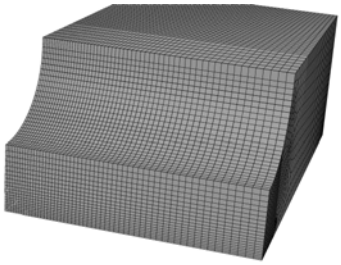
Fig. 10 *X-TF* History for *FN*-11, *FN*-14 and *FN*-17 specimens shown on *X-TF* plane with nearest high sensitivity regions taken from Fig. 9. For $TF_{,1}$ diagram, there is no high sensitivity region for $\sigma_{eq} / \sigma_1 \geq 0.5$



(a)



(b)



(c)

Fig. 11 Mesh of *FN* specimens at convergence; *FN*-11, *FN*-14 and *FN*-17 respectively. One eight of the specimens are modeled and failure occurs where three symmetry planes meet

https://doi.org/10.1017/jmech.2012.125 Published online by Cambridge University Press

Table 4 Averaged X and TF for two different mesh sizes

specimen	Mesh size > 0.1mm		Mesh size < 0.1mm		difference	
	TF_{avg}	X_{avg}	TF_{avg}	X_{avg}	TF_{avg}	X_{avg}
FN-11	1.38	0.2	1.38	0.2	0	0
FN-14	1	0.12	1.03	0.13	0.03	0.01
FN-17	1.18	0.08	1.21	0.12	0.03	0.04

6. CONCLUSIONS

TF and X are two parameters that have effect on failure strain. From finite element-experimental analysis it is shown that increasing TF_{avg} decreases failure strain and decreasing X_{avg} decreases failure strain. Moreover an equation is developed for failure strain.

The sensitivity analysis shows that these two parameters are severely sensitive to stress deviations for example in some cases a deviation of 5% in one of principal stresses, causes 20% ~ 30% deviation in X and 15% ~ 20% deviation in TF. Therefore special attention should be paid to large deformation elastoplastic analyses which are done for calculating these parameters both in element size and step size. Mesh sensitivity based on stresses may cause some severe errors in calculating these parameters and element sizes in failure area should be reduced lower than the values reported in literature.

REFERENCES

1. Bridgman, P. W., *Studies in Large Plastic Flow and Fracture with Special Emphasis on the Effects of Hydrostatic Pressure*, First Edition, McGraw-Hill, New York (1952).
2. Lemaitre, J., "A Continuous Damage Mechanics Model for Ductile Fracture," *Journal of Engineering Materials Technology*, **107**, pp. 83–89 (1985.).
3. Lemaitre, J., Desmorat, R. and Sausay, M., "Anisotropic Damage Laws of Evolution," *European Journal of Mechanics*, **19**, pp. 187–208 (2000).
4. Chaboche, J. L., "Continuous Damage Mechanics: A Tool to Describe Phenomena Before Crack Initiation," *Nuclear Engineering and Design*, **64**, pp. 233–247 (1981).
5. Bao, Y., "Prediction of Ductile Crack Formation in Uncracked Bodies," Ph.D Thesis, Department of Mechanics Engineering, MIT, U.S.A. (2003).
6. Xue, L. and Wierzbicki, T., "Ductile Fracture Initiation and Propagation Modeling Using Damage Plasticity Theory," *Engineering Fracture Mechanics*, **75**, pp. 3276–3293 (2008).
7. Bai, Y. and Wierzbicki, T., "A New Model of Metal Plasticity and Fracture with Pressure and Lode Dependence," *International Journal of Plastics*, **24**, pp. 1071–1096 (2008).
8. Gao, X., Zhang, T., Hayden, M. and Roe, C., "Effects of the Stress State on Plasticity and Ductile Failure of an Aluminum 5083 Alloy," *International Journal of Plastics*, **25**, pp. 2366–2382 (2009).
9. Mirone, G. and Corallo, D., "A Local Viewpoint for Evaluating the Influence of Stress Triaxiality and Lode Angle on Ductile Failure and Hardening," *International Journal of Plastics*, **26**, pp. 348–371 (2010).
10. Wierzbicki, T., Bao, Y., Lee, Y. W. and Bai, Y., "Calibration and Evaluation of Seven Fracture Models," *International Journal of Mechanical Sciences*, **47**, pp. 719–743 (2005).
11. Barsoum, I. and Faleskog, J., "Micromechanical Analysis on the Influence of the Lode Parameter on Void Growth and Coalescence," *International Journal of Solids and Structures*, **48**, pp. 925–938.
12. Barsoum, I. and Faleskog, J., "Rupture Mechanisms in Combined Tension and Shear– Micromechanics," *International Journal of Solids and Structures*, **44**, pp. 5481–5498.
13. Coppola, T., Corallo, D. and Mirone, G., "Determinazione Della Curva Costitutiva Postnecking Per Metalli Duttili," *Proceedings of 38th National Conference of AIAS – Italian Association for Stress Analysis*, Italy (2009).
14. Mirone, G., Keshavarz, A. and Ghajar, R., "An Experimental Failure Model Based on Triaxiality Factor and Lode Angle for X-100 Pipeline Steel," *Proceedings of X-Mech-2012*, Iran (2012).
15. Broggiato, G. B., Coppola, T. and Cortese, L., "Caratterizzazione Sperimentale Del Legame Elasto-Plastico Ad Elevate Deformazioni Mediante La Prova Di Torsione," *Proceedings of 39th Conference of AIAS – Italian Association for Stress Analysis*, Italy (2010).
16. Mirone, G., "A New Model for the Elastoplastic Characterization and the Stress–Strain Determination on the Necking Section of a Tensile Specimen," *International Journal of Solids and Structures*, **41**, pp. 3545–3564 (2004).
17. Bai, Y., "Effect of Loading History on Necking and Fracture," Ph. D. Thesis, Department of Mechanics Engineering, MIT, U.S.A. (2008).
18. Coppola, T., Cortese, L. and Folgarati, P., "The Effect of Stress Invariants on Ductile Fracture Limit in Steels," *Engineering Fracture Mechanics*, **76**, pp. 1288–1302 (2009).
19. Hashemi, S. H., Howard, I. C., Yates, J. R. and Andrews, R. M., "The Transferability of Micro Mechanical Damage Parameters in Modern Pipeline Steel," *15th Europian Conference on Fracture*, Sweden (2004).
20. Hashemi, S. H., Howard, I. C., Yates, J. R. and Andrews, R. M., "Micromechanical Damage Modelling of Notched Bar Testing of Modern Line Pipe Steel," *15th Europian Conference on Fracture*, Sweden (2004).

(Manuscript received February 15, 2012, accepted for publication May 8, 2012.)

https://doi.org/10.1017/jmech.2012.125 Published online by Cambridge University Press